Deep–Sea Research II 194 (2021) 104998

Contents lists available at ScienceDirect

Deep-Sea Research Part II

journal homepage: www.elsevier.com/locate/dsr2

Evaluation and projection of global marine heatwaves based on CMIP6 models

Zijian Qiu [a,b], Fangli Qiao [b,c], Chan Joo Jang [d], Lujun Zhang [a], Zhenya Song [b,c,*]

[a] School of Atmospheric Sciences, Nanjing University, Nanjing, 210023, China
[b] First Institute of Oceanography, and Key Laboratory of Marine Science and Numerical Modeling, Ministry of Natural Resources, Qingdao, 266061, China
[c] Laboratory for Regional Oceanography and Numerical Modeling, Pilot National Laboratory for Marine Science and Technology, Qingdao, 266237, China
[d] Ocean Circulation Research Center, Korea Institute of Ocean Science and Technology, Busan, 49111, South Korea

ARTICLE INFO

Keywords:
Marine heatwaves
Extreme event
Climate change
CMIP6

ABSTRACT

Marine heatwaves (MHWs) are extreme climatic events that last for days to months and can extend up to thousands of kilometers and cause substantial ecological, social, and economic impacts. Climate models are the key tool for studying and predicting MHWs. However, it continues to be challenging for climate models to accurately simulate MHWs. In this study, we evaluate 29 models from the Coupled Model Intercomparison Project Phase 6 (CMIP6) and 19 models from the Coupled Model Intercomparison Project Phase 5 (CMIP5) in terms of their capabilities to simulate MHWs by examining the spatial patterns and temporal variations. Then, we estimate future changes until the end of the 21st century under three shared socioeconomic pathways (SSPs) (e.g., SSP126, SSP245, and SSP585). The results show that the CMIP6 ensemble mean is more skillful in capturing the features of MHWs than that of the CMIP5. The biases of the CMIP6 models for the MHWs intensities are within ±0.5 °C over most of the oceans, except in the western boundary current regions and eastern tropical Pacific, where the modeled MHWs are up to 1.5 °C weaker than the observations. In comparison, the results from CMIP5 are greater than ±1.5 °C in most areas. Both the CMIP5 and CMIP6 models underestimate long-duration MHWs in the eastern tropical Pacific, where they are nearly 20 days shorter than the observations. In most areas, the CMIP5 models overestimate the MHWs durations (by over 25 days), while the biases of the CMIP6 models are within 10 days. The projected MHWs exhibit significant increases in the intensity and duration and reach maximum intensities of 4 °C. The largest changes are projected to occur in the tropics, North Pacific, and North Atlantic. When comparing the shared socioeconomic pathways for the increasing trend of MHWs, the most extreme MHWs occur under SSP585, with their intensities nearly doubling and a near-permanent MHWs state occurring by the 2070s.

1. Introduction

The oceans are warming significantly, and temperature extremes are increasing globally (Cheng et al., 2019), which lead to increase in the intensities and durations of marine heatwaves (MHWs) (Hobday et al., 2016). MHWs can last for days to months and can extend up to thousands of kilometers (Oliver et al., 2018). These extreme events threaten marine ecosystems, cause mass mortality events, species range shifts and community reconfigurations (Lonhart et al., 2019; Smale et al., 2019). Studies have documented the ecological and social impacts of recent MHWs, including coral bleaching (Leggat et al., 2019), massive die-offs of marine invertebrates (Carneiro et al., 2020; Harvell et al., 2019), extinction of bull kelp (Thomsen et al., 2019), and fishery closures or quota changes (Caputi et al., 2016; Oliver et al., 2017).

MHWs are the direct results of local-scale processes, such as ocean heat advection, air-sea interaction, and vertical mixing (Amaya et al., 2020; Di Lorenzo and Mantua, 2016; Schmeisser et al., 2019), and act within the mixed layer (Holbrook et al., 2019), which can be modulated by remote influences (such as El Niño-Southern Oscillation, ENSO) via teleconnections (Oliver et al., 2018; Yao et al., 2020).

Climate models are important tools for studying and predicting MHWs. Based on the experimental results of the global climate models (GCMs) that were provided by the Coupled Model Intercomparison Project (CMIP), previous studies have shown that MHWs have become

* Corresponding author. First Institute of Oceanography, and Key Laboratory of Marine Science and Numerical Modeling, Ministry of Natural Resources, No. 6 Xian-Xia-Ling Road, Qingdao, 266061, China.
E-mail address: songroy@fio.org.cn (Z. Song).

https://doi.org/10.1016/j.dsr2.2021.104998
Received 13 July 2021; Received in revised form 22 October 2021; Accepted 8 November 2021
Available online 11 November 2021

longer and more frequent over the past century and are projected to continue to increase under global warming (Frölicher et al., 2018; Hayashida et al., 2020; Oliver et al., 2019; Plecha and Soares, 2020; Yao et al., 2020). However, it continues to be a challenge for climate models to accurately simulate MHWs. Studies on the global (Oliver et al., 2019) and regional (Darmaraki et al., 2019; Plecha et al., 2021) MHWs mean properties show that CMIP5 tends to simulate less frequent, weaker, and longer-lasting MHWs than the observations, and there are many differences among the models. This bias can be attributed to the limitations due to coarse resolution (Pilo et al., 2019) because coarse-resolution models underestimate the SST anomalies in eddy-rich regions.

Currently, the CMIP has entered its sixth phase (CMIP6), with generally higher spatial resolutions and improved parameterization schemes for major physical processes than its CMIP5 counterpart (Taylor et al., 2012; Eyring et al., 2016). Researchers have recently started to analyze MHWs with the new CMIP6 results. Plecha and Soares, 2020 evaluated the simulation abilities of 16 CMIP6 models and analyzed future MHWs changes. However, they mainly used coarse-resolution model outputs to simulate the MHWs, and their evaluation focused on the ensemble mean results.

Do high-resolution CMIP6 models provide more confidence than CMIP5 in simulating MHWs on a global scale? To answer this question, we evaluate 29 models from CMIP6, which include high-resolution and coarse-resolution models, and 19 models from CMIP5 for their simulations of MHWs. Then, we analyze whether the model abilities for simulating MHWs have improved by comparing the results of the CMIP6 and CMIP5 models from the same model groups. In addition, the SS score (Pierce et al., 2009) and M2 score (Chen et al., 2011) methods are used to quantify the model abilities from the aspects of spatial patterns and temporal variation, which provide a reference to improve the credibility of future forecasts. Based on this, we estimate the future changes until the end of the 21st century under three shared socioeconomic pathways (e.g., SSP126, SSP245, and SSP585).

2. Data and methodology

2.1. Observational and model datasets

To evaluate the model performances over a historical period, we use the daily SST field from the 1/4° NOAA OI SST V2 dataset over 1982–2015 (Reynolds et al., 2007). This dataset has been widely used to analyze MHWs worldwide. Compared with the coarse-resolution models, the satellite data are regridded onto a regular 1° × 1° grid before calculating the MHWs metrics.

We examined the daily SST outputs of 29 CMIP6 models (Table 1) and 19 CMIP5 models (Table 2). All of the historical SST data cover the same period from 1982 to 2015. The SST data for 5 selected models that were used in the analysis of future projections cover the period of 2016–2100. Three future scenarios are considered that follow SSP126, SSP245, and SSP585. These models are selected based on the availability of daily SST data of ensemble member *r1i1p1*. We also use the preindustrial control simulations of 7 models (e.g., CMCC-CM2-SR5, HadGEM3-GC31-LL, MRI-ESM2-0, NorESM2-LM, ACCESS-ESM1-5, and IPSL-CM6A-LR), which represent historical conditions without anthropogenic influences.

We calculate the MHWs metrics for each model on its native grid and then interpolate the output to a regular 1° by 1° grid to calculate the multimodel ensemble (MME).

2.2. MHWs definition

We calculate MHWs from the daily SST fields following the definition that was developed to facilitate comparisons among studies (Hobday et al., 2016). A MHWs event was defined as a discrete prolonged anomalously warm water event when the daily SSTs exceed the 90th percentile for five consecutive days or more based on a 30-year historical time series. The 90th percentile and daily climatology are calculated for each calendar day by using the daily SSTs within an 11-day window

Table 1
The basic information, SS score, and M2 score for 29 CMIP6 models. The associated institutions and countries, names, and resolution of each model are shown. The table also lists the rankings of the SS scores and M2 scores.

Model center, Country	Model	Resolution	SS score (No.)		M2 score (No.)	
			total days	intensity	total days	intensity
CSIRO(Australia)	ACCESS-CM2	300 × 360	0.06(13)	−0.05(11)	1.84(19)	0.82(18)
CSIRO(Australia)	ACCESS-ESM1-5	300 × 360	−0.4(21)	−0.24(21)	2.18(22)	0.69(16)
BCC(China)	BCC-ESM1	232 × 360	−0.58(26)	−0.00(9)	0.93(14)	0.64(13)
	BCC-CSM2-MR	232 × 360	−0.63(27)	−0.00(9)	0.83(12)	0.64(13)
CCCma(Canada)	CanESM5	360 × 291	−0.45(23)	−0.10(14)	2.24(23)	0.02(1)
NCAR(USA)	CESM2-FV2	384 × 320	−0.78(28)	−0.21(20)	2.36(24)	2.08(22)
	CESM2-WACCM	384 × 320	−0.43(22)	−0.34(25)	2.14(21)	0.21(7)
CMCC(Italy)	CMCC-CM2-HR4	1442 × 1051	0.24(7)	0.3(4)	0.86(13)	0.24(8)
	CMCC-CM2-SR5	292 × 360	0.38(2)	−0.16(17)	0.41(5)	0.15(5)
	CMCC-CM2-VHR4	1442 × 1051	0.14(10)	0.34(2)	0.98(15)	2.92(24)
EC(European)	EC-Earth3-Veg	292 × 362	−0.04(16)	0.05(8)	0.79(10)	1.56(21)
ECMWF(European)	ECMWF-IFS-HR	1021 × 1051	0.21(8)	0.100(7)	2.76(26)	2.28(23)
	ECMWF-IFS-LR	292 × 362	−0.19(19)	−0.21(19)	0.82(11)	0.07(4)
CAS(China)	FGOALS-f3-L	218 × 360	0.25(6)	−0.4(27)	1.07(16)	0.15(6)
FIO-QLNM(China)	FIO-ESM-2-0	384 × 320	0.30(4)	−0.18(18)	0.08(4)	0.56(12)
NOAA-GFDL(USA)	GFDL-CM4	1080 × 1440	0.15(9)	0.42(1)	0.02(1)	0.69(15)
MOHC(UK)	HadGEM3-GC31-LL	330 × 360	−0.81(29)	−0.52(28)	12.85(28)	75.87(28)
	HadGEM3-GC31-MM	1220 × 1440	−0.57(25)	−0.6(29)	14.81(29)	87.33(29)
IPSL(France)	IPSL-CM6A-LR	332 × 362	−0.15(18)	0.17(6)	4.20(27)	3.85(25)
MIROC(Japan)	MIROC6	256 × 360	0.05(14)	−0.39(26)	1.81(18)	0.72(17)
MPI-M(Germany)	MPI-ESM1-2-LR	220 × 256	0.11(12)	−0.12(16)	0.47(6)	0.51(11)
	MPI-ESM1-2-HR	404 × 802	−0.04(15)	−0.05(12)	0.05(3)	0.33(9)
	MPI-ESM1-2-XR	404 × 802	−0.09(17)	−0.11(15)	0.03(2)	0.05(3)
MRI(Japan)	MRI-ESM2-0	363 × 360	0.29(5)	−0.33(24)	0.63(8)	0.03(2)
NCAR(USA)	NCAR-CESM2	384 × 320	−0.57(24)	−0.30(23)	2.39(25)	0.49(10)
NUIST(China)	NESM3	292 × 362	0.11(11)	0.33(3)	0.59(7)	1.26(20)
NCC (Norway)	NorESM2-LM	360 × 385	0.60(1)	0.19(5)	0.66(9)	7.11(27)
	NorESM2-MM	360 × 385	0.35(3)	−0.07(13)	2.11(20)	4.41(26)
SNU(Korea)	SAM0-UNICON	384 × 320	−0.2(20)	−0.27(22)	1.35(17)	0.90(19)
CMIP6 MME			0.40	0.22	0.2	0.04

Table 2
Same as Table 1 but based on CMIP5.

Model center, Country	Model	Resolution	SS score (No.)		M2 score (No.)	
			total days	Intensity	total days	intensity
CSIRO-BOM(Austrialia)	ACCESS1-0	300 × 256	0.035(2)	−0.41(12)	0.39 (9)	0.39 (9)
	ACCESS1-3	300,360	0.039(1)	−0.38(10)	0.56 (11)	0.62 (13)
CCCma(Canada)	Can-ESM2	192 × 256	−0.01(5)	−0.48(14)	1.16 (15)	1.01 (16)
CMCC(Italy)	CMCC-CESM	148 × 182	−0.13(13)	−0.44(13)	0.32 (8)	0.93 (15)
	CMCC-CM	148 × 180	−0.07(8)	−0.50(15)	0.03 (2)	0.18 (5)
	CMCC-CMS	148 × 180	−0.10(10)	−0.40(11)	0.85 (14)	0.38 (8)
CSIRO-QCCCE(Austrialia)	CSIRO-Mk3-6-0	96 × 192	−0.32(18)	−0.53(16)	0.02 (1)	0.24 (6)
CAS(China)	FGOALS-g2	196 × 360	−0.32(18)	−0.70(17)	0.07 (3)	0.12 (4)
FIO(China)	FIO-ESM	384 × 320	−0.06(7)	−0.76(18)	0.13 (6)	0.11 (3)
NOAA-GFDL(USA)	GFDL-CM3	200 × 360	−0.03(6)	−0.11(6)	0.18 (7)	0.43 (10)
	GFDL-ESM2G	210 × 360	−0.28(15)	0.58(1)	0.70 (12)	0.05 (2)
MOHC(UK)	HadCM2	144 × 288	−0.3(17)	0.38(4)	2.82 (17)	2.98 (17)
	HadFEM2-CC	216 × 360	−0.10(10)	0.37(5)	2.73 (16)	3.75 (18)
	HadFEM2-ES	216 × 360	−0.07(8)	0.40(3)	4.04 (19)	4.78 (19)
IPSL(France)	IPSL-CM5A-LR	149 × 182	−0.10(10)	−0.27(9)	0.47 (10)	0.56 (11)
MIROC(Japan)	MIROC5	224 × 256	−0.19(14)	−0.80(19)	3.99 (18)	0.59 (11)
MPI-M(Germany)	MPI-ESM-LR	220 × 256	−0.28(15)	0.43(2)	0.78 (13)	0.63 (14)
MRI(Japan)	MRI-CGCM3	168 × 360	0.13(3)	−0.14(8)	0.12 (5)	0.01 (1)
	MRI-ESM1	368 × 360	0.09(4)	−0.12(7)	0.09 (4)	0.28 (7)
CMIP5 MME			−0.11	−0.20	1.02	0.95

that were smoothed by applying a 31-day moving average. Events with gaps of two days or fewer are considered to be continuous events. A seasonally varying threshold enables the detection of MHWs at any time of the year rather than detecting events that occur only during the warmest months.

The 90th percentile is determined based on a common period of 1982–2005. This fixed historical baseline for MHWs evaluations and projections is consistent with previous studies (Hayashida et al., 2020; Oliver et al., 2019; Plecha and Soares, 2020) and is useful for analyzing their impacts on ecosystems that cannot adapt to rapid warming rates.

While some studies have used other percentile ranks (Darmaraki et al., 2019; Frölicher and Laufkötter, 2018) or have advocated the use of a moving baseline threshold (Jacox, 2019), by referring to the previous research, we noticed that the threshold definition depends on the specific scientific problem in question (Oliver et al., 2019). In addition, changing the thresholds did not change the conclusions regarding the increases in MHWs in future projections (Hayashida et al., 2020).

The MHWs definition does not consider the effects of sea ice. Therefore, we limit our analysis to between 70°S and 50°N. To characterize MHWs, we calculate the time series of the total number of days (the number of MHWs days in a year) and intensities (average of the temperature anomalies overall MHWs events in a year relative to the seasonal climatology) for each year.

2.3. Metric evaluation of datasets

The model performances in simulating spatial patterns are evaluated using the SS score method (Pierce et al., 2009). The SS score can be defined as:

$$SS = 1 - \frac{MSE(m,o)}{MSE(\overline{o},o)} \tag{1}$$

$$MSE = (\overline{m} - \overline{o})^2 + s_m^2 + s_o^2 - 2s_m s_o r_{m,o} \tag{2}$$

where MSE is the mean squared error, m(x) is the model output, o(x) are the observations, overbars indicate spatial averages, $r_{m,o}$ is the product-moment spatial correlation coefficient between the model and observations, and s_m and s_o are the spatial standard deviations of the model and observations, respectively. A model field that is identical to the observations has a skill score of 1.

The score can be decomposed as:

$$SS = r_{m,o}^2 - \left[r_{m,o} - (s_m - s_o)\right]^2 - \left[(\overline{m} - \overline{o})/_{s_o}\right]^2 \tag{3}$$

The first term on the right-hand side of Eq. (3) is the square of the pattern correlation. The second term is the "conditional bias", which expresses a model that over- or underpredicts excursions. The third term is the "unconditional bias", which is the square of the mean error that is normalized by the standard deviation of the observations. This decomposition helps us to better describe the pattern bias.

The performance of a dataset in simulating the interannual variations in the MHWs metrics is evaluated by using the M2 score (Chen et al., 2011), which is defined as follows:

$$M2 = \left(\frac{STD_m}{STD_o} - \frac{STD_o}{STD_m}\right)^2 \tag{4}$$

where STD_m denotes the interannual standard deviation of the simulation and STD_o is the STD of the observation. The $M2$ value is equal to 0 when the STD_m is identical to the STD_o, and the closer the $M2$ value is to 0, the greater the skill in simulating the interannual variability. After obtaining the SS and M2 scores for each CMIP6 and CMIP5 model, the simulation ability rankings of the models are shown in Tables 1 and 2, respectively.

The overall performance of the CMIP6 models is evaluated by plotting a scatter diagram of the M2 values against the SS scores.

3. Results

3.1. Evaluation of CMIP6 models and comparison with CMIP5 models

To evaluate the capability of models in simulating the MHWs metrics over the globe, Fig. 1 shows the biases between the models and observations in the historical periods (e.g., CMIP5:1982–2005, CMIP6:1982–2015).

Both the CMIP6 MME and CMIP5 MME overestimate the total days in the southern and equatorial Pacific Oceans, where MHWs last more than 10 days in the CMIP6 MME and 25 days in the CMIP5 MME. The CMIP5 MME shows nearly 20 days of negative bias in the subtropical Indian, Pacific, and Atlantic Oceans.

The intensities of the CMIP6 models have a general cold bias worldwide. Large cold biases are located in the western boundary current region and eastern equatorial Pacific Ocean, where the local bias is as high as 2 °C. Compared with the CMIP5 MME, this bias is lower in the

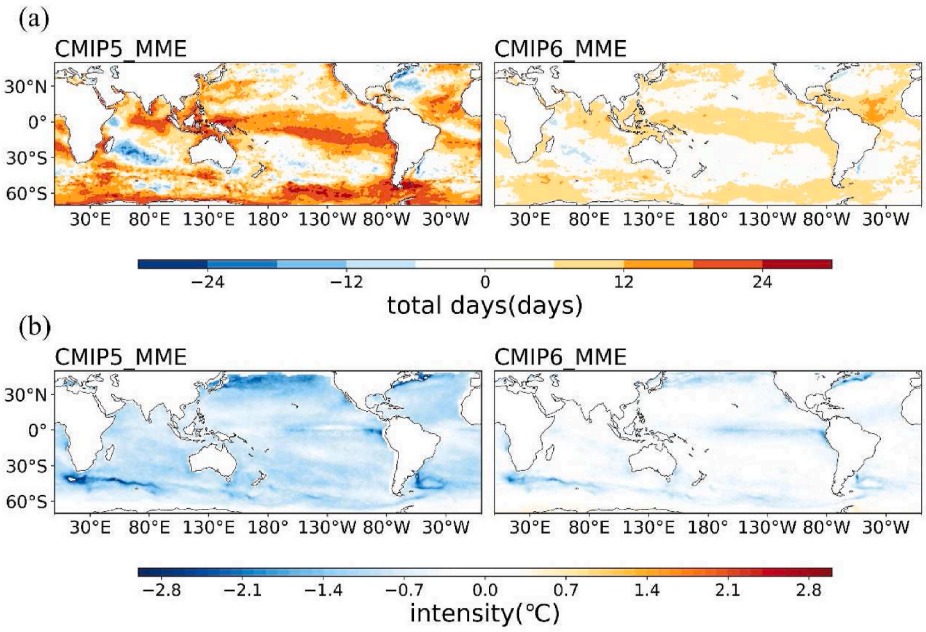

Fig. 1. Spatial distributions of model biases (e.g., MMEs minus observations). (a) Total number of days, and (b) intensity of MHWs. MME means multi-model ensemble.

CMIP6 MME.

The scatter diagram in Fig. 2 quantitatively demonstrates the similarities of the MHWs spatial patterns between the models and observations. The result from the MME is better than those from individuals. The majority of the CMIP6 models have pattern correlations greater than 0.7 for the total days and intensities of MHWs, which indicate that the model can simulate the spatial distributions of the heatwave characteristics. However, most models overestimate the total days of MHWs (Fig. S1a), although the biases are smaller in models CMCC-CM-HR4, EC-Earth3-Veg, ECMWF-IFS-HR, FGOALS-F3-L, GFDL-CM4, MPI-ESM1-2-HR, NESM3, and Nor-ESM2-MM. Most models have standard deviations that are smaller than 1, which indicate underestimated intensities, while HadGEM3-GC21-LL, HadGEM3-GC21-MM, and NESM3 have positive biases (Fig. S1b). Some studies consider this bias to be linked to a persistent positive downward energy flux bias in ocean surface warming, which may be related to a shortcoming of the cumulus convection parameterization scheme (Plecha and Soares, 2020).

We also compare several groups of models from the same research institution that participated in both the CMIP5 and CMIP6. Most CMIP5 models also overestimate the total days (Fig. S2a) and underestimate the intensities (Fig. S2b), but their pattern correlations are lower than those of the CMIP6 models (Fig. 2). HadGEM2-CC and HadGEM2-ES have visible positive biases for the intensities, which are similar to HadGEM3-GC21-LL and HadGEM3-GC21-MM. In general, the results show that the simulation abilities of the CMIP6 models are improved compared to those of CMIP5.

As illustrated in Fig. 3, the linear MHWs trends that are obtained from the MMEs of the two CMIPs are similar. The observation data show a positive trend for the total number of days. From 1982 to 2020, the total number of days grew at a rate of 10.7 days per decade. The total number days increased at a rate of 15.9 days per decade in the CMIP6 MME and 16.3 days in the CMIP5 MME, which are much more than

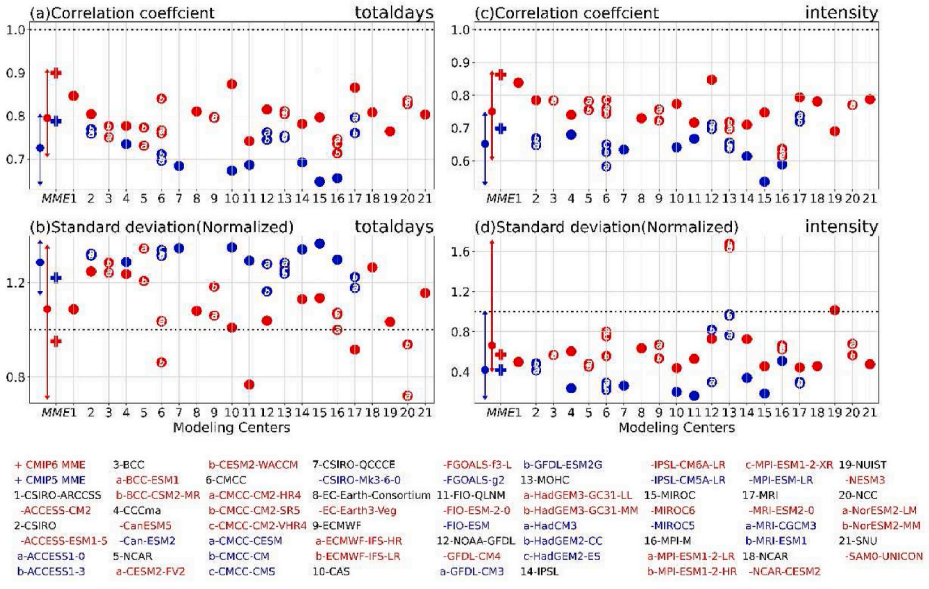

Fig. 2. Scatter diagram of the pattern correlation coefficients and normalized standard deviations. (a) (b) Total number of days, and (c) (d)intensity. The red dots represent CMIP6 models, and the blue dots represent CMIP5 models. The cross symbols indicate multimodel ensembles (MME). The red and blue error bars show the means and upper and lower limits of all CMIP6 and CMIP5 models, respectively. The horizontal dashed lines indicate a value of 1. Thus, those models that lie close to these lines have good performance in simulating the climatology of the indices.

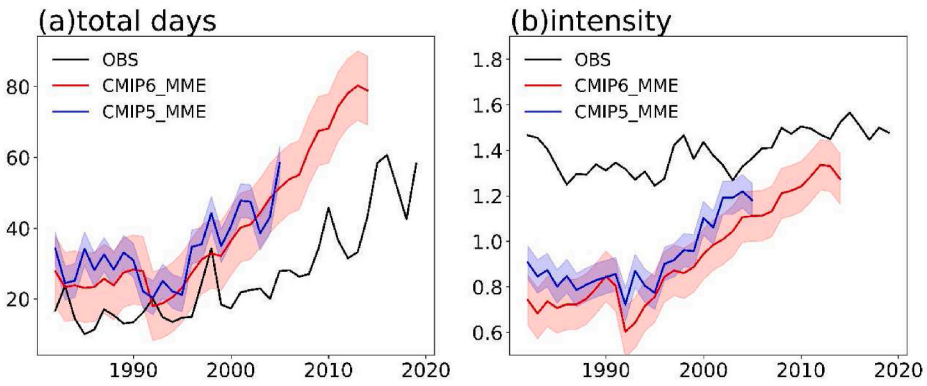

Fig. 3. Time evolution graphs of the MHWs metrics. (a) Total days, and (b) intensity. The red lines represent CMIP6 MME, the blue lines represent CMIP5 MME, and the black lines are the observations. The shaded represents 0.5 times the intermodal standard deviation.

those shown by the observations. There was a rapid rise after 2000 in the models, while the observations increased steadily. For the intensities, the models underestimated the values but overestimated the linear trends by four-fold compared to the observations. The intensities that were estimated by the observations showed a trend of 0.05 °C per decade, which resulted in an increase of 0.2 °C in the last 30 years. On the other hand, the CMIP5 MME and CMIP6 MME results have significant growth rates of 0.19 and 0.22 °C per decade, respectively.

The SS and M2 scores are also used to further evaluate the overall model abilities to simulate the spatial patterns and interannual variations in the MHWs indices (listed in Table 1). Fig. 4 shows scatter diagrams of the SS scores versus M2 scores, where the horizontal and vertical lines are the median score values, respectively. A model that plots below the horizontal line or to the right of the vertical line has better performance than the median of the overall model performances in reproducing the spatial patterns or interannual variations. Thus, the models in the green shaded quadrant can accurately capture the climatology and interannual variations of the MHWs metrics. The results show that CMCC-CM2-HR4, CMCC-VHR4, FIO-ESM-2-0, GFDL-CM4, and MPI-ESM1-2-HR have good performance in simulating the MHWs characteristics. As the CMP6 models have better performace than CMIP5 models, we use CMIP6 models to project the MHWs future changes under SSP126, SSP245, and SSP585.

We compared the durations and intensities of the MHWs of 5 selected model simulations and the remaining 24 model simulations with the observations. Fig. S3 shows the spatial distributions of the biases between the models and observations. The ensemble result of the 5 selected models shows smaller biases in the Indian Ocean, west subtropical Pacific Ocean, and Southern Ocean, both for the MHWs intensity and total number of days. These 5 models simulate the intensities more precisely, especially in the western boundary current region, such as in the region of the Agulhas Current, where the negative biases are generally less than 0.5 °C. As shown in Fig. S4, the total number of days increases at a rate of 11.2 days per decade in these 5 model ensembles and 16.8 days per decade in the remaining 24 model ensembles, which are 0.5 days and 8.3 days longer than the observations, respectively. For the intensity simulations, these 5 models also underestimate the intensities but show growth rates of 0.12 °C per decade, which are closer to the observations (0.05 °C). These 5 model ensembles simulate the MHWs more accurately than the others, so we use them to estimate and

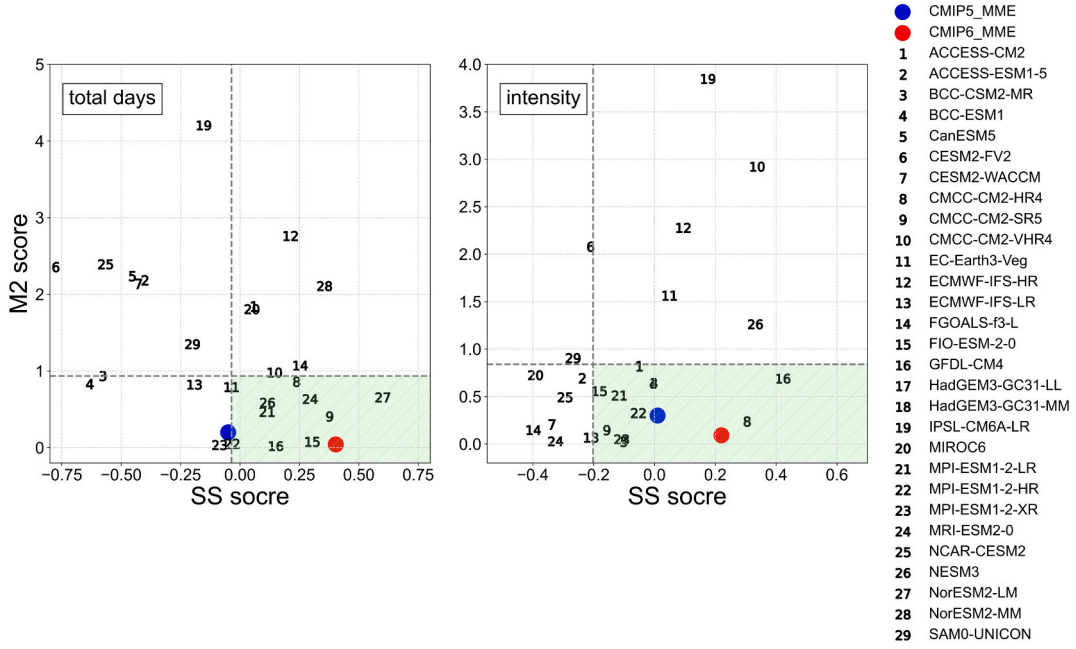

Fig. 4. Scatter diagram of the model climate performance index (SS score) versus the model variability index (M2 score) for MHWs; (a) the total number of days and (b) intensity. The horizontal and vertical dashed lines are the median SS and M2 values. Thus, the models that lie in the bottom right quadrant (green shaded zone) have better performance than the median in simulating both the climatology and interannual variations of the indices.

project future MHWs up to 2100.

3.2. Future projections

We consider three scenarios, namely, SSP126, SSP245, and SSP585, to estimate the future changes until the end of the 21st century by using the selected models that accurately simulate MHWs. The projected MHWs show an increase in total days and intensities during the 21st century.

The spatial distributions of the increased rates (fold) of MHWs in 2071–2100 relative to the historical period (1982–2015) are shown in Fig. 5. The increases in total days are concentrated in the Southern Ocean and subtropical Pacific in the SSP126 and SSP245 scenarios. In the SSP585 scenario, there will be extremely long MHWs in most areas at the end of the century, which increase by ten times compared to the historical period and even reach a "permanent MHWs state" .

MHWs were significantly intense during the historical period in the western boundary current regions and eastern equatorial Pacific Ocean (Fig. S1b). As shown in Fig. 5, the spatial distributions of the changes suggest intensity increases for nearly the entire study area under the three scenarios. The areas of increase are located in the Southern Ocean and eastern equatorial Pacific Ocean, where the intensities are nearly 600% of those in the historical period.

The total MHWs days show positive trends of 10.6 days, 29.2 days, and 45.9 days per decade under the three scenarios (Fig. 6a). The severities of the SSPs influence the linear trends. In the SSP585 experiment, the globe is projected to reach a "permanent MHWs state" (365 days per year, Fig. 6a, horizontal dashed line) at the end of the century. It is also projected that the total number of days will extend beyond the range of natural variability by 2047 under SSP126, 2039 under SSP245, and 2039 under SSP585.

The intensities are projected to increase significantly for both SSP245 and SSP585, and the trends are 0.10 °C and 0.19 °C, respectively. These changes are mainly related to the changes in the mean values rather than changes in the variations (Oliver et al., 2019a; Plecha and Soares, 2020). Importantly, the intensity series exceeds the range of natural variability in 2035 under SSP245 and 2024 under SSP585. However, the increase in the SSP126 scenario is not obvious, nor does it completely exceed the range of the natural variations.

4. Discussion and conclusions

In this study, we use 29 CMIP6 models to simulate MHWs for a historical period and compare them with 19 CMIP5 models. Then, we select 5 models with better simulation performances to analyze the future changes until 2100 under future scenarios.

Similar to previous work based on CMIP models or high-resolution ocean circulation models, we also noticed that the MHWs have exhibited a positive linear trend in recent years and continue to grow in future projections.

In the historical period, the CMIP5 and CMIP6 MMEs share common shortcomings in the simulations. As in previous studies based on the CMIP5 models and observations, it is indicated that the biases, where the models simulated longer and weaker MHWs, are consistent with the limitations due to coarse resolution (Oliver et al., 2019; Darmaraki et al., 2019). Specifically, the models underestimate the SST anomalies that are produced by mesoscale processes and simulate SST time series that are much too smooth, particularly in the western boundary current area and Southern Ocean. Plecha et al. (2021) mentioned the persistence of this limitation in the new-generation CMIP6 models.

To determine the possible influence of model resolution on simulating the spatial patterns of MHWs, we plot the SS and M2 scores against the model resolution (Fig. 7a, b, c, d). The results indicate that the model resolutions and SS scores for the intensities have relatively positive correlations. The models with a nominal ocean resolution of 25 km performed better, and three models (e.g., NESM3, IPSL-CM6A-LR, and Nor-ESM2-LM) with lower resolution also obtained good scores. We decompose the SS scores for intensity into the correlations, conditional biases, and unconditional biases (Fig. 7e, f, g). The SS scores are mainly affected by unconditional biases in this case, which describe the differences in the spatial averages between the models and observations. Most models underestimate the MHWs intensities, especially in the western boundary current and eastern equatorial Pacific Ocean. Models including NESM3, IPSL-CM6A-LR, and Nor-ESM2-LM have a warm bias in the Indian Ocean and subtropical Pacific, which partially offsets the negative bias, which results in good spatial skill scores. Models with high resolution, such as GFDL-CM4, CMCC-CM2-HR4, CMCC-CM2-VHR4, and ECMWF-IFS-HR, have slight cold biases in the area of the western boundary current. In fact, when comparing models from the same institute (Fig. 2), we found that the high-resolution models performed better than the lower resolution models. We plan to carry out comparative experiments and attempt to investigate the specific mechanisms by which the model resolution affects the simulation capabilities for the MHWs in our future work.

The projections for future MHWs reveal that there will be longer and more intense MHWs over the 21st century, which are consistent with the

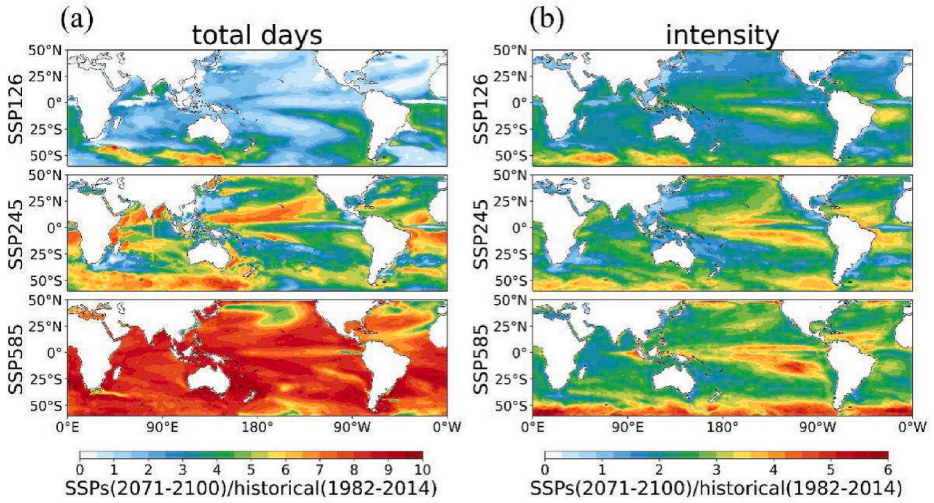

Fig. 5. Spatial distributions of the increased rate (fold) of MHWs at the end of the 21st century (2071–2100) relative to the historical period; (a) total number of days and (b) intensity.

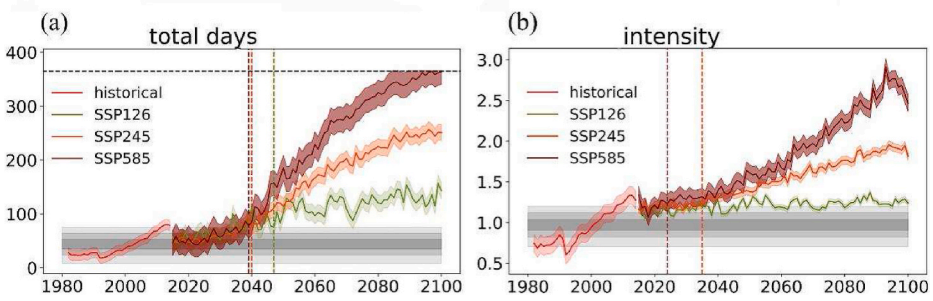

Fig. 6. Global average time series of MHWs metrics under the SSP126 (green), SSP245 (orange), and SSP585 (red) scenarios; (a) total number of days and (b) intensity. The gray shaded region shows the range of natural variability based on the preindustrial run and its range of ±1, ±2, and ±3.5 standard deviations. The vertical dashed line represents the year that the signals extend beyond the natural internal variations. We used 29 CMIP6 models to analyze the MHWs in the historical period and 5 selected models to estimate the future changes under three scenarios, so the series were discontinuous in 2015 and 2016.

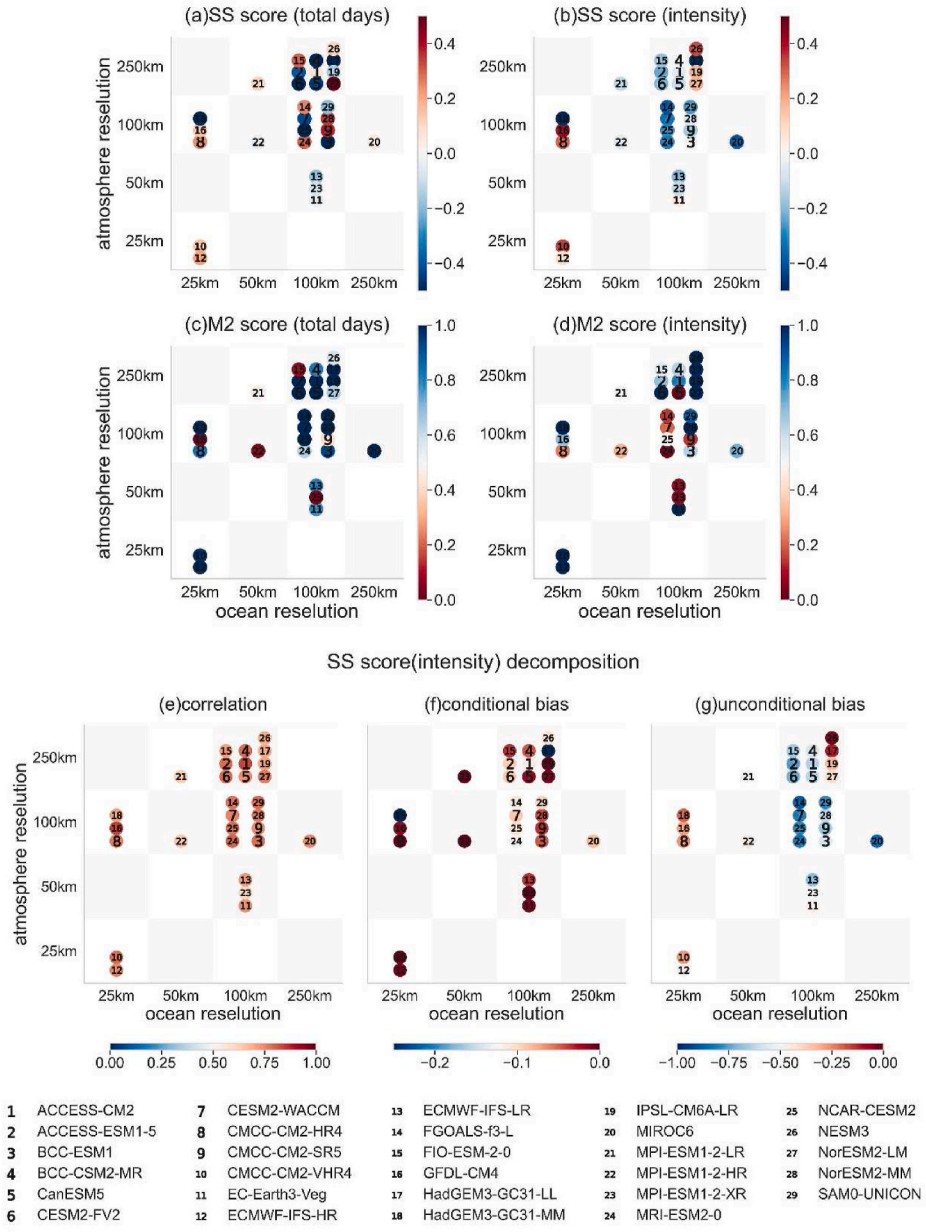

Fig. 7. Schematics showing the SS and M2 scores at ocean and atmospheric resolutions; (a) SS scores for total days, (b) SS scores for intensity, (c) M2 scores for total days, and (d) M2 scores for intensity. The colors correspond to the values. The SS scores for intensity are decomposed into three terms: (e) correlation, (f) conditional bias, and (g) unconditional bias.

results of previous studies (Oliver et al., 2019; Plecha and Soares, 2020).

Different emission scenarios influence the projected MHWs. The estimated increase in the MHWs intensity and duration under SSP585 by 2100 (compared with the historical period for 1982–2015) nearly triples compared to that under SSP126. Our work suggests that anthropogenic influences will accelerate the growth of MHWs. The emergence of a

permanent MHWs state implies that the historical "extreme" conditions might no longer be "extreme" in the future, and would indicate that the ocean has entered a brand-new state. Severe MHWs will become powerful and cause disturbances to marine ecosystems in the near future (Frölicher et al., 2018; Hayashida et al., 2020; Oliver et al., 2019; Plecha and Soares, 2020; Yao et al., 2020).

In summary, the simulation abilities of most CMIP6 models, especially the high-resolution models, has improved relative to their CMIP5 counterparts. Meanwhile, the CMIP6 models still face ground challenges. Improving the ability of models to simulate MHWs by using either higher-resolution GCMs or regional coupled models, especially new parameterizations, is crucial. The projected MHWs are increasingly longer and more severe and will become serious global issues or ground challenges that need to be addressed from a global perspective.

CRediT author statement

All authors jointly conceived the study and contributed equally to the experimental data. Zijian Qiu: Data curation, Visualization, Writing-Original draft preparation. Fangli Qiao: Design, Writing-Review & Editing, Supervision; ChanJoo Jang: Validation, Writing-Review & Editing; Lujun Zhang: Validation, Writing-Review & Editing; Zhenya Song: Conceptualization, Writing-Review & Editing, Supervision.

Declaration of competing interest

The authors declare that they have no known competing financial interests or personal relationships that could have appeared to influence the work reported in this paper.

Acknowledgments

We thank the climate modeling groups for producing and making available their model outputs, the Earth System Grid Federation (ESGF) for archiving and providing access to the data, and the multiple funding agencies who support CMIP and ESGF. All CMIP data are available from the ESGF at https://esgf-data.dkrz.de/search/cmip5-dkrz/and https://esgf-data.dkrz.de/search/cmip6-dkrz/. The NOAA OI SST v2 dataset was obtained from PSL/NOAA (https://psl.noaa.gov/data/gridded/data.noaa.oisst.v2.highres.html). This work is supported by the National Key R&D Program of China (Grants 2017YFC1404000), National Natural Science Foundation of China (42022042 and 41821004), China-Korea Cooperation Project on Northwestern Pacific Climate Change and its Prediction, and CAS Interdisciplinary Innovation Team (JCTD-2020-12).

Appendix A. Supplementary data

Supplementary data to this article can be found online at https://doi.org/10.1016/j.dsr2.2021.104998.

References

Amaya, D.J., Miller, A.J., Xie, S.-P., Kosaka, Y., 2020. Physical drivers of the summer 2019 North Pacific marine heatwave. Nat. Commun. 11, 1903. https://doi.org/10.1038/s41467-020-15820-w.

Caputi, N., Kangas, M., Denham, A., Feng, M., Pearce, A., Hetzel, Y., Chandrapavan, A., 2016. Management adaptation of invertebrate fisheries to an extreme marine heat wave event at a global warming hot spot. Ecol Evol 6, 3583–3593. https://doi.org/10.1002/ece3.2137.

Carneiro, A.P., Soares, C.H.L., Manso, P.R.J., Pagliosa, P.R., 2020. Impact of marine heat waves and cold spell events on the bivalve Anomalocardia flexuosa: a seasonal comparison. Mar. Environ. Res. 156, 104898. https://doi.org/10.1016/j.marenvres.2020.104898.

Chen, W., Jiang, Z., Li, L., 2011. Probabilistic projections of climate change over China under the SRES A1B scenario using 28 AOGCMs. J. Clim. 24, 4741–4756. https://doi.org/10.1175/2011JCLI4102.1.

Cheng, L., Abraham, J., Hausfather, Z., Trenberth, K.E., 2019. How fast are the oceans warming? Science 363, 128–129. https://doi.org/10.1126/science.aav7619.

Darmaraki, S., Somot, S., Sevault, F., Nabat, P., Cabos Narvaez, W.D., Cavicchia, L., Djurdjevic, V., Li, L., Sannino, G., Sein, D.V., 2019. Future evolution of marine heatwaves in the mediterranean sea. Clim. Dynam. 53, 1371–1392. https://doi.org/10.1007/s00382-019-04661-z.

Di Lorenzo, E., Mantua, N., 2016. Multi-year persistence of the 2014/15 North Pacific marine heatwave. Nat. Clim. Change 6, 1042–1047. https://doi.org/10.1038/nclimate3082.

Eyring, V., Bony, S., Meehl, G.A., Senior, C.A., Stevens, B., Stouffer, R.J., Taylor, K.E., 2016. Overview of the coupled model Intercomparison project phase 6 (CMIP6) experimental design and organization. Geosci. Model Dev. (GMD) 9, 1937–1958. https://doi.org/10.5194/gmd-9-1937-2016.

Frölicher, T.L., Fischer, E.M., Gruber, N., 2018. Marine heatwaves under global warming. Nature 560, 360–364. https://doi.org/10.1038/s41586-018-0383-9.

Frölicher, T.L., Laufkötter, C., 2018. Emerging risks from marine heat waves. Nat. Commun. 9, 650. https://doi.org/10.1038/s41467-018-03163-6.

Harvell, C.D., Montecino-Latorre, D., Caldwell, J.M., Burt, J.M., Bosley, K., Keller, A., Heron, S.F., Salomon, A.K., Lee, L., Pontier, O., Pattengill-Semmens, C., Gaydos, J.K., 2019. Disease epidemic and a marine heat wave are associated with the continental-scale collapse of a pivotal predator (*Pycnopodia helianthoides*). Sci. Adv. 5, eaau7042 https://doi.org/10.1126/sciadv.aau7042.

Hayashida, H., Matear, R., Strutton, P., Zhang, X., 2020. Insights into projected changes in marine heatwaves from a high-resolution ocean circulation model. Nat. Commun. 11, 4352. https://doi.org/10.1038/s41467-020-18241-x.

Hobday, A.J., Alexander, L.V., Perkins, S.E., Smale, D.A., Straub, S.C., Oliver, E.C.J., Benthuysen, J.A., Burrows, M.T., Donat, M.G., Feng, M., Holbrook, N.J., Moore, P.J., Scannell, H.A., Sen Gupta, A., Wernberg, T., 2016. A hierarchical approach to defining marine heatwaves. Prog. Oceanogr. 141, 227–238. https://doi.org/10.1016/j.pocean.2015.12.014.

Holbrook, N.J., Scannell, H.A., Sen Gupta, A., Benthuysen, J.A., Feng, M., Oliver, E.C.J., Alexander, L.V., Burrows, M.T., Donat, M.G., Hobday, A.J., Moore, P.J., Perkins-Kirkpatrick, S.E., Smale, D.A., Straub, S.C., Wernberg, T., 2019. A global assessment of marine heatwaves and their drivers. Nat. Commun. 10, 2624. https://doi.org/10.1038/s41467-019-10206-z.

Jacox, M.G., 2019. Marine heatwaves in a changing climate. Nature 571, 485–487. https://doi.org/10.1038/d41586-019-02196-1.

Leggat, W.P., Camp, E.F., Suggett, D.J., Heron, S.F., Fordyce, A.J., Gardner, S., Deakin, L., Turner, M., Beeching, L.J., Kuzhiumparambil, U., Eakin, C.M., Ainsworth, T.D., 2019. Rapid coral decay is associated with marine heatwave mortality events on reefs. Curr. Biol. 29, 2723–2730. https://doi.org/10.1016/j.cub.2019.06.077 e4.

Lonhart, S.I., Jeppesen, R., Beas-Luna, R., Crooks, J.A., Lorda, J., 2019. Shifts in the distribution and abundance of coastal marine species along the eastern Pacific Ocean during marine heatwaves from 2013 to 2018. Mar. Biodivers Rec. 12, 13. https://doi.org/10.1186/s41200-019-0171-8.

Oliver, E.C.J., Benthuysen, J.A., Bindoff, N.L., Hobday, A.J., Holbrook, N.J., Mundy, C. N., Perkins-Kirkpatrick, S.E., 2017. The unprecedented 2015/16 Tasman Sea marine heatwave. Nat. Commun. 8, 16101. https://doi.org/10.1038/ncomms16101.

Oliver, E.C.J., Burrows, M.T., Donat, M.G., Sen Gupta, A., Alexander, L.V., Perkins-Kirkpatrick, S.E., Benthuysen, J.A., Hobday, A.J., Holbrook, N.J., Moore, P.J., Thomsen, M.S., Wernberg, T., Smale, D.A., 2019. Projected marine heatwaves in the 21st century and the potential for ecological impact. Front. Mar. Sci. 6, 734. https://doi.org/10.3389/fmars.2019.00734.

Oliver, E.C.J., Donat, M.G., Burrows, M.T., Moore, P.J., Smale, D.A., Alexander, L.V., Benthuysen, J.A., Feng, M., Sen Gupta, A., Hobday, A.J., Holbrook, N.J., Perkins-Kirkpatrick, S.E., Scannell, H.A., Straub, S.C., Wernberg, T., 2018. Longer and more frequent marine heatwaves over the past century. Nat. Commun. 9, 1324. https://doi.org/10.1038/s41467-018-03732-9.

Yao, Y., Wang, J., Yin, J., Zou, X., 2020. Marine heatwaves in China's marginal seas and adjacent offshore waters: past, present, and future. J. Geophys. Res. Oceans 125, e2019JC015801. https://doi.org/10.1029/2019JC015801.

Pierce, D.W., Barnett, T.P., Santer, B.D., Gleckler, P.J., 2009. Selecting global climate models for regional climate change studies. Proc. Natl. Acad. Sci. Unit. States Am. 106, 8441–8446. https://doi.org/10.1073/pnas.0900094106.

Pilo, G.S., Holbrook, N.J., Kiss, A.E., Hogg, A.McC., 2019. Sensitivity of marine heatwave metrics to ocean model resolution. Geophys. Res. Lett. 46, 14604–14612. https://doi.org/10.1029/2019GL084928.

Plecha, S.M., Soares, P.M.M., 2020. Global marine heatwave events using the new CMIP6 multi-model ensemble: from shortcomings in present climate to future projections. Environ. Res. Lett. 15, 124058. https://doi.org/10.1088/1748-9326/abc847.

Plecha, S.M., Soares, P.M.M., Silva-Fernandes, S.M., Cabos, W., 2021. On the uncertainty of future projections of marine heatwave events in the North Atlantic Ocean. Clim. Dynam. 56, 2027–2056. https://doi.org/10.1007/s00382-020-05529-3.

Reynolds, R.W., Smith, T.M., Liu, C., Chelton, D.B., Casey, K.S., Schlax, M.G., 2007. Daily high-resolution-blended analyses for sea surface temperature. J. Clim. 20, 5473–5496. https://doi.org/10.1175/2007JCLI1824.1.

Schmeisser, L., Bond, N.A., Siedlecki, S.A., Ackerman, T.P., 2019. The role of clouds and surface heat fluxes in the maintenance of the 2013–2016 northeast pacific marine heatwave. J. Geophys. Res. Atmos. 124, 10772–10783. https://doi.org/10.1029/2019JD030780.

Smale, D.A., Wernberg, T., Oliver, E.C.J., Thomsen, M., Harvey, B.P., Straub, S.C., Burrows, M.T., Alexander, L.V., Benthuysen, J.A., Donat, M.G., Feng, M., Hobday, A. J., Holbrook, N.J., Perkins-Kirkpatrick, S.E., Scannell, H.A., Sen Gupta, A., Payne, B. L., Moore, P.J., 2019. Marine heatwaves threaten global biodiversity and the

provision of ecosystem services. Nat. Clim. Change 9, 306–312. https://doi.org/10.1038/s41558-019-0412-1.

Taylor, K.E., Stouffer, R.J., Meehl, G.A., 2012. An overview of CMIP5 and the experiment design. Bull. Am. Meteorol. Soc. 93, 485–498. https://doi.org/10.1175/BAMS-D-11-00094.1.

Thomsen, M.S., Mondardini, L., Alestra, T., Gerrity, S., Tait, L., South, P.M., Lilley, S.A., Schiel, D.R., 2019. Local extinction of bull kelp (durvillaea spp.) due to a marine heatwave. Front. Mar. Sci. 6, 84. https://doi.org/10.3389/fmars.2019.00084.